Research Article

Screening and identification of HTNV$_{pv}$ entry inhibitors with high-throughput pseudovirus-based chemiluminescence

Xiaojing Wen [a,b,1], Li Zhang [a,1], Qiang Liu [a], Xinyue Xiao [c], Weijin Huang [a,*], Youchun Wang [a,*]

[a] *Division of HIV/AIDS and Sex-transmitted Virus Vaccines, Institute for Biological Product Control, National Institutes for Food and Drug Control (NIFDC) and WHO Collaborating Center for Standardization and Evaluation of Biologicals, Beijing 102629, China*
[b] *Department of Microbiological Laboratory Technology, School of Public Health, Shandong University, Jinan 250012, China*
[c] *Institute for Reference Standards and Standardization, National Institutes for Food and Drug Control, Beijing 102629, China*

ABSTRACT

Hantaviruses, such as Hantaan virus (HTNV) and Seoul virus, are the causative agents of Hantavirus cardiopulmonary syndrome (HCPS) and hemorrhagic fever with renal syndrome (HFRS), and are important zoonotic pathogens. China has the highest incidence of HFRS, which is mainly caused by HTNV and Seoul virus. No approved antiviral drugs are available for these hantaviral diseases. Here, a chemiluminescence-based high-throughput-screening (HTS) assay was developed and used to screen HTNV pseudovirus (HTNV$_{pv}$) inhibitors in a library of 1813 approved drugs and 556 small-molecule compounds from traditional Chinese medicine sources. We identified six compounds with *in vitro* anti-HTNV$_{pv}$ activities in the low-micromolar range (EC$_{50}$ values of 0.1–2.2 μmol/L; selectivity index of 40–900). Among the six selected compounds, cepharanthine not only showed good anti-HTNV$_{pv}$ activity *in vitro* but also inhibited HTNV$_{pv}$-fluc infection in Balb/c mice 5 h after infection by 94% (180 mg/kg/d, $P < 0.01$), 93% (90 mg/kg/d, $P < 0.01$), or 92% (45 mg/kg/d, $P < 0.01$), respectively, in a bioluminescent imaging mouse model. A time-of-addition analysis suggested that the antiviral mechanism of cepharanthine involves the membrane fusion and entry phases. Overall, we have established a HTS method for antiviral drugs screening, and shown that cepharanthine is a candidate for HCPS and HFRS therapy. These findings may offer a starting point for the treatment of patients infected with hantaviruses.

1. Introduction

Hantaan virus (HTNV) was discovered in the late 1970s (Montoya-Ruiz et al., 2014), and belongs to the genus *Orthohantavirus* of the family *Hantaviridae*. It is an important zoonotic pathogen that infects humans and small rodents. HTNV is an enveloped negative-stranded RNA virus with a genome that includes three fragments: L, M, and S, which encode the L polymerase, Gn and Gc glycoproteins, and nuclear proteins, respectively. It can cause both Hantavirus cardiopulmonary syndrome (HCPS) and hemorrhagic fever with renal syndrome (HFRS) (Milholland et al., 2018; Tian and Stenseth, 2019). In some outbreaks, the mortality rate of HCPS has been as high as 50%. Hantavirus infection is a global disease, with more than 150,000 HFRS patients worldwide each year, and about 90% of reported cases occurred in China (Jonsson et al., 2010). Hantaviruses can be divided into more than 30 genotypes or serotypes, among which Hantaan virus (HTNV) and Dobrava-Belgrade virus have

the highest mortality rates in the HFRS-affected population of up to 15% (Kariwa et al., 2007; Avsic-Zupanc et al., 2019). Patients with HTNV are predominantly found in East Asia (Llah et al., 2018). Its pathogenesis may be a complex multifactorial process. There is currently only supportive, but not specific treatment for HFRS caused by HTNV. Studies have shown that ribavirin can inhibit the replication of HTNV *in vitro*, and it has shown some effects in mouse experiments. But when the disease progresses to the cardiopulmonary phase, ribavirin has no inhibitory effect (Brocato and Hooper, 2019). Therefore, there is an urgent need to develop or discover highly effective and low-toxicity anti-HTNV drugs.

The development of new antiviral drugs is time-consuming and expensive, with low returns. Therefore, investigating the antiviral functions of approved drugs, i.e., drug repurposing, may be more effective than the development of new drugs. Advantage can be taken of the known pharmacological and toxicity profiles of approved drugs, their established safety in humans, and the proven feasibility of their

* Corresponding authors.
  E-mail addresses: huangweijin@nifdc.org.cn (W. Huang), wangyc@nifdc.org.cn (Y. Wang).
[1] Xiaojing Wen and Li Zhang contributed equally to this work.

manufacture and formulation. This strategy also has other advantages, such as the low risk of failure, short development time, and low cost etc (Mercorelli et al., 2018; Pushpakom et al., 2019; Sohraby et al., 2017).

Hantaviruses belong to the class of highly pathogenic microorganisms that must be studied in a biosafety level 3 (BSL-3) laboratory. This entails great inconvenience for the researcher. To address this restriction, we previously developed a replication-defective, vesicular stomatitis virus (VSV)-based pseudovirus expressing HTNV glycoprotein (GP), and demonstrated the utility of this pseudovirus in both high-throughput screening (HTS) *in vitro* and in a bioluminescent imaging (BLI) mouse model (Zhang et al., 2017). Importantly, this pseudoviral system can be safely used in BSL-2 laboratories.

In this study, a chemiluminescence-based HTS assay was developed to identify antiviral inhibitors of the HTNV pseudovirus ($HTNV_{pv}$). We screened a library of 1813 U.S. Food and Drug Administration (FDA)-approved drugs and 556 small-molecule compounds from traditional Chinese medicine sources. Six compounds were identified as having antiviral effects against $HTNV_{pv}$ (half-maximal effective concentration [EC_{50}] values of 0.1–2.2 μmol/L and selectivity index [SI] of 40–900). Cepharanthine (CEP) not only showed good anti-HTNV activity *in vitro*, but also inhibited HTNV-fluc infection in Balb/c mice 5 h after infection, by 94% (180 mg/kg/d, $P < 0.01$), 93% (90 mg/kg/d, $P < 0.01$), or 92% (45 mg/kg/d, $P < 0.01$), respectively, in the BLI mouse model.

2. Materials and methods

2.1. Cell lines, pseudovirus and authentic virus

Vero E6 cells (ATCC® CRL-1586) were cultured under 5% CO_2 at 37 °C in high-glucose Dulbecco's modified Eagle's medium (DMEM, HyClone, South Logan, UT) supplemented with 10% fetal bovine serum (Gibco, Carlsbad, CA), 1% penicillin–streptomycin solution (Gibco), and 2% 4-(2-hydroxyethyl)-1-piperazineethanesulfonic acid (Gibco). The cells were passaged every 2–3 days.

The ORF of codon-optimized versions of HTNV (76–118 strain), including *Gn* and *Gc* genes was added to the pcDNA3.1(+) vector. The glycoprotein was autocleaved to Gn and Gc after expression. The detailed procedure was described in our previously published paper (Ning et al., 2021).

The VSV-based HTNV pseudovirus ($HTNV_{pv}$) expressing HTNV GP and the firefly luciferase reporter protein (Fluc) was constructed and stored in our laboratory. Briefly, HEK293T cells were plated one day before transfection. When cells reached 70%–90% confluence, the culture medium was discarded. 48 μg (for T150 flask) of the GP expression plasmid was transfected according to the instructions of Lipofectamine 3000 (Invitrogen). Cells were infected with 5.1×10^6 median tissue culture infective doses ($TCID_{50}$) G*ΔG-VSV virus (VSV G pseudotyped virus, Kerafast) at the same time. The cell medium was discarded 6–8 h after transfection and infection. The cells were gently washed three times with PBS and cultured in fresh complete DMEM at 37 °C with 5% CO_2. Twenty-four hours later, the culture supernatant containing $HTNV_{pv}$ was harvested, filtered, aliquoted, and frozen at −70 °C for further use.

Authentic virus HTNV (76–118 strain) was from the Department of Arboviral Vaccine, Institute for Biological Product Control, National Institutes for Food and Drug Control.

2.2. Compound library

The 1813 FDA-approved drug compounds were purchased from TargetMol (Shanghai, China). The 556 small-molecule compounds from traditional Chinese medicine sources were provided by the National Standard Chemical Control Library of NIFDC (National institutes for Food and Drug Control, Beijing, China). These compounds were dissolved in dimethyl sulfoxide (DMSO; Sigma-Aldrich, St. Louis, MO) at a concentration of 10 mmol/L and stored at −80 °C until use.

2.3. Screening assay with pseudovirus

In the first round of HTS, Vero E6 cells were seeded in 96-well plates (Corning, Inc., Corning, NY) at a density of 3×10^4 cells/well. After incubation overnight, the cells were treated in duplicate with 10 μmol/L compounds. The cells were then incubated at 37 °C under 5% CO_2 for 1 h, and 50 μL of $HTNV_{pv}$ was added to each well. The luciferase activity was measured 23 h later. In short, 100 μL of culture medium was aspirated gently from the cells and 100 μL of Bright-Glo® Luciferase reagent (Promega, Madison, WI) was added to each well and allowed to react with the cells for 2 min at room temperature. The luminescence was measured with a GloMax® 96 Microplate Luminometer (Promega). The percentage inhibition was calculated as (1 − relative light units [RLU] in the presence of compound −RLU of negative control)/(RLU of positive control − RLU of negative control) × 100. The primary positive compounds were identified by their apparent lack of cytotoxicity and their reduction of adenoviral replication by > 50% in duplicate wells at a concentration of 10 μmol/L. The EC_{50} of each compound was determined from a dose–response curve of $HTNV_{pv}$ at eight serially diluted doses (30 μmol/L, 10 μmol/L, 3.3 μmol/L, and 1.1 μmol/L, 0.4 μmol/L, 0.1 μmol/L, 0.03 μmol/L and 0.01 μmol/L) in the second screening.

2.4. Cytotoxicity assay

Cytotoxicity was tested with the CellTiter-Glo® Luminescent Cell Viability Assay (Promega) to determine the 50% cytotoxic concentration (CC_{50}) of each test compound in the absence of pseudovirus. Serial dilutions of the drugs (90–0.04 μmol/L) were mixed with Vero E6 cells in 96-well plates, and 50 μL of complete medium was added instead of virus. After incubation at 37 °C under 5% CO_2 for 24 h, cell viability was measured with the GloMax® 96 Microplate Luminometer.

2.5. Animal experiments

The mice were handled in accordance with the institutional (NIFDC) guidelines for laboratory animal care and use, and the Animal Care and Use Committee at NIFDC approved the study protocol. Female Balb/c mice (4–5 weeks old; n = 5 per group) were obtained from the Institute for Laboratory Animal Resources of NIFDC. Compounds were dissolved in 0.5% methylcellulose (Sigma-Aldrich). To challenge the mice, 4.2×10^5 $TCID_{50}$ of p/VSV/HVGP/Fluc was delivered by intraperitoneal (IP) injection to the groups of five mice. Different CEP doses (180, 90, or 45 mg/kg) were administered to each group. The times of administration were 6 h before infection and 2 h after infection.

The BLI analysis was performed with the IVIS Lumina Series III Imaging System (PerkinElmer, Baltimore, MD), as previously described (Zhang et al., 2017). The Living Image software (Caliper Life Sciences, Baltimore, MD) was used to analyze the regions of interest. The data are presented as the total fluxes in photons/s.

2.6. Time of addition

A time-of-addition experiment was performed to evaluate the antiviral mechanism of CEP (Basu et al., 2011). Vero E6 cells were seeded in 96-well plates 1 day in advance of virus infection. The cells were incubated with 30 μmol/L CEP for 1 h before infection (−1 h, 4 °C), during infection (0 h, 37 °C), and 1 h after infection (1 h, 37 °C). Six duplicate wells were assigned to each time point. The control infected-cell cultures were treated with the drug vehicle (DMSO) only. At 24 h post infection, the cells were harvested and the infectivity was measured as described above.

2.7. Authentic HTNV infection and nucleic acid detection

Vero E6 cells were pre-seeded into 24 well plates (2×10^5/well) one day before the infection. HTNV (76–118 strain) was added to the culture

supernatant at the MOI of 0.3, 0.003 or 0.00075. The same amount of diluted CEP was added to the experiment and mock cells at a concentration of 20 μmol/L or serially diluted (20 μmol/L, 6.66 μmol/L, and 2.22 μmol/L). After 36 h, the medium was discarded. Cells were washed with PBS for three times. The nucleic acid was extracted with Qiagen kit (QIAamp Viral RNA Mini Kit, 52904). The fluorescence quantitative PCR amplification was performed with nucleic acid detection kit for hemorrhagic fever with renal syndrome virus (Beijing BGI-GBI-biotech Co., China). Inhibition efficacy was calculated as the following formula: $100 \times [1 - (\text{RLU in the presence of compound} - \text{RLU of cells control})/(\text{RLU of virus control} - \text{RLU of cells control})]$.

2.8. Statistical analysis

GraphPad Prism 6 (San Diego, CA) was used to analyze the EC_{50} and CC_{50} values of the compounds and the BLI data. Statistical comparisons were made with a t-test. P values of <0.05 were considered statistically significant. $*P < 0.05$, $**P < 0.01$, $***P < 0.005$, and $****P < 0.001$, ns, $P > 0.05$.

3. Results

3.1. Identification of $HTNV_{pv}$ entry inhibitors with an in vitro pseudovirus screen

A pseudovirus containing a firefly luciferase reporter gene enveloped by HTNV glycoprotein G was used for HTS to select inhibitors of viral entry from a library of 1813 approved drugs and 556 small-molecule compounds derived from traditional Chinese medicine sources. This system can be safely used in BSL-2 environments to generate high titers of replication-incompetent pseudovirus, which can then be used in combination with highly sensitive luciferase reporter assays for HTS. The HTS schema is shown in Fig. 1A. The HTS conditions, including the cell-seeding density and $HTNV_{pv}$ dose, were optimized to 30,000 cells/well and 2000 $TCID_{50}$/well, respectively. Under these conditions, the signal-to-basal (S/B) ratio, the coefficient of variation (CV), and the Z′ factor were 826, 10%, and 0.69, respectively (Fig. 1B). These data indicate that the experiment met the HTS requirements (Zhang et al., 1999; Zhang et al., 2006). The plate layout for the HTS screening was shown in Fig. 1C. The primary screen was performed with a single dose (10 μmol/L) of each compound to identify those with activity against $HTNV_{pv}$. The results indicated that 74 hit compounds had $>50\%$ inhibitory activity, thus necessitating a second round of screening.

Because compounds inhibiting VSV replication or luciferase activity will also inhibit $HTNV_{pv}$, VSV_{pv} expressing an unrelated VSV envelope

glycoprotein was tested in parallel in the second round of screening. Each of the 74 compounds was diluted in a 1:3 ratio to generate four concentrations, ranging from 30 μmol/L to 0.01 μmol/L, to confirm their activity against $HTNV_{pv}$ and VSV_{pv}, and to determine their EC_{50} values. When the EC_{50} VSV_{pv}/EC_{50} $HTNV_{pv}$ ratio was >3, the compound was deemed to be positive. As a result, 12 compounds were confirmed to block $HTNV_{pv}$-mediated infection, with little effect on VSV_{pv} infection. The evaluation of both the antiviral activity and the cytotoxicity of the compounds was critical because cytotoxic compounds can appear to exert antiviral activity when the cellular inhibition assay is largely dependent on cell viability.

The 12 hit compounds identified in the counterscreen were further evaluated in parallel for their cytotoxicity in uninfected Vero E6 cells, using eight-point dose–response curves (starting from 90 μmol/L) to determine their EC_{50} values for $HTNV_{pv}$ and their CC_{50} values. The ratio of CC_{50} to EC_{50} for $HTNV_{pv}$ was calculated as SI. Many compounds were not tested at high enough concentrations to accurately determine their SI values, but compounds with anti-$HTNV_{pv}$ activities < 3-fold greater than their cytotoxicities were much less likely to be useful antiviral compounds *in vivo*.

After the final confirmatory screening, six hit compounds were identified as efficacious against $HTNV_{pv}$ with low cytotoxicity, with SI values of >40 (Table 1, Fig. 2). Among the six hit drugs, mycophenolate mofetil (MMF) with the highest SI value, and mycophenolic acid are immunosuppressants. MMF is also reported to have broad-spectrum antiviral activity (Ye et al., 2012; Cho et al., 2017). Whereas MLN9708 and MLN2238 are proteasome inhibitors, cepharanthine is a SARS coronavirus (SARS-CoV) inhibitor and toosendanin is an influenza virus inhibitor (Wang et al., 2016; Augello et al., 2018; Jin et al., 2019).

3.2. Confirmation of $HTNV_{pv}$ inhibitors with an in vivo BLI model

To test whether the antiviral activity of the active compounds observed *in vitro* can be translated to enhanced activity against $HTNV_{pv}$ infection *in vivo*, we evaluated the treatment effects of the six compounds identified with HTS. Because MMF is a derivative of MPA, only MPA but not MMF was selected for the experiment. Totally five compounds were used in the experiment. First, the five compounds (90 mg/kg/day) were delivered by IP injection to Balb/c mice before infection (-6 h). The mice were then infected intraperitoneally with 4.2×10^5 $TCID_{50}$ $HTNV_{pv}$ (0 h). The five compounds were then re-administered 2 h after infection. The BLI analysis showed that one of the five compounds (CEP) reduced $HTNV_{pv}$ infection. The inhibitory effect is presented as the percentage reduction in the BLI signal compared with that in the control group (Fig. 3A). The mice in the groups treated with other three drugs
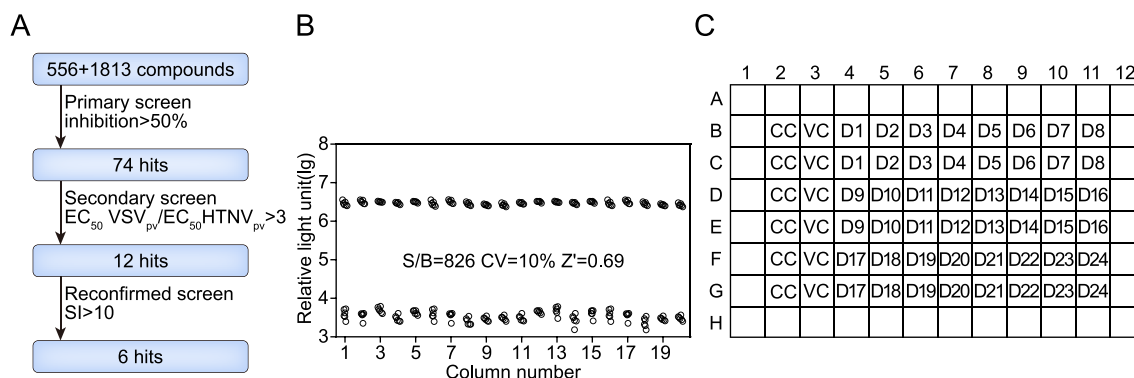

Fig. 1. High-throughput screening (HTS) for inhibitors of HTNV *in vitro*. **A** Flow chart of HTS assay using $HTNV_{pv}$. **B** Scatterplot of the results of DMSO plate screening. The 96-well assay plates contained Vero E6 cells in one column was divided into two groups, half with only cells as the cell control (0% response), the other half was cells added with $HTNV_{pv}$ as the Virus control (positive control, 100% response). 20 columns of data were summarized here. The signal-to-basal (S/B) ratio = mean signal/mean background, Z′ factor = 1- 3SD of sample + 3SD of control/(mean of sample - mean of control). **C** Layout of *in vitro* screening. CC, cell control (0% response), VC, virus control (positive control, 100% response), D1–D24, Drug1–24.

Table 1

In vitro anti-HTNVpv activity of six hit compounds.

Compound Name	EC_{50}[a]-$HTNV_{pv}$ (µmol/L)	EC_{50}-VSV (µmol/L)	CC_{50}[b] (µmol/L)	SI^c=CC_{50}/IC_{50}	VSV/$HTNV_{pv}$	Pharmacological classes
Mycophenolate Mofetil	0.1	0.6	>90	>900	6.0	Immunosuppressant (Hong et al. 2022)
MLN9708	0.2	2.4	>90	>450	12.0	Proteasome inhibitor (Engur-Ozturk and Dikmen, 2022)
Mycophenolic acid	0.2	0.6	>90	>450	3.0	Immunosuppressant (Yap et al. 2022)
MLN2238	0.2	1.7	>90	>450	8.5	proteasome inhibitor (Grad et al. 2021)
cepharanthine	0.9	7.0	49.5	50	7.8	SARS inhibitor (Zhang et al. 2005)
toosendanin	2.2	7.7	>90	>40	3.5	Influenza virus inhibitor (Jin et al. 2019)

HTNVpv, Pseudotyped Hantaan virus.

[a] EC_{50}: 50% effective concentration. It was determined with an inhibition assay in Vero E6 cells infected with $HTNV_{pv.}$ The values presented are the averages of three experiments.

[b] CC_{50}: 50% cytotoxic concentration. It was determined with the CellTiter-Glo Luminescent Cell Viability Assay.
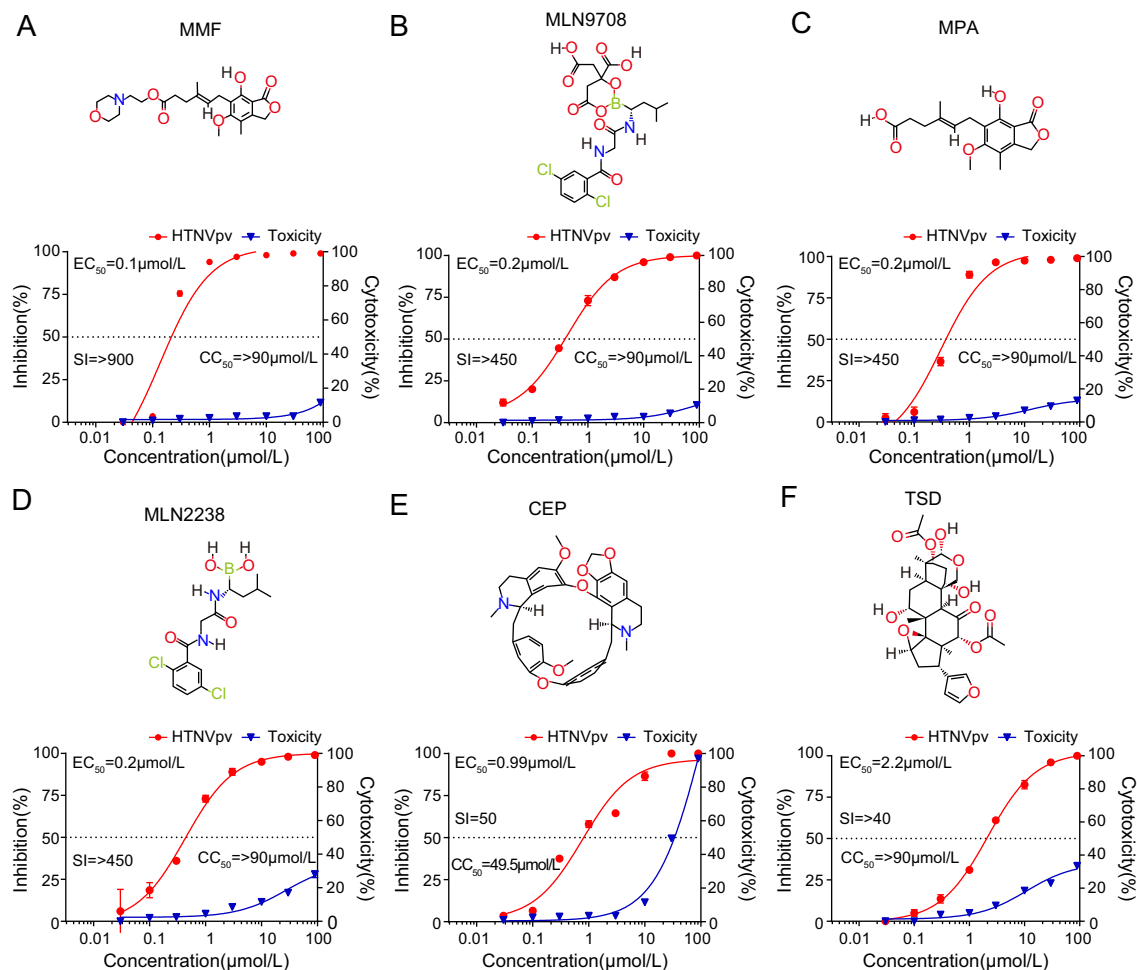
[c] SI: Selectivity index: CC_{50}/EC_{50}.

Fig. 2. Effect of six compounds on $HTNV_{pv}$ *in vitro*. **A** MMF, **B** MLN9708, **C** MPA, **D** MLN2238, **E** CEP, **F** TSD. The chemical structural formulas of compounds are presented. Antiviral activities of $HTNV_{pv}$ and cytotoxicity to Vero E6 cells of each compound are analyzed. Data represents mean ± SEM. The experiments were repeated three times. Abbreviations: CEP, cepharanthine; MPA, mycophenolic acid; MMF, mycophenolate mofetil; TSD, toosendanin; HTNV, hantana virus.

(MLN9708, MLN2238, and toosendanin) were not shown due to premature mortality, which caused the death of the mice. The experiment with CEP was repeated with three different doses, 180, 90, or 45 mg/kg/day (totally equivalent to 3.0, 1.5 or 0.75 mg/mice in this study), which produced obvious inhibitory effects, with inhibitory rates of 94% ($P <$ 0.01), 93% ($P <$ 0.01), and 92% ($P <$ 0.01), respectively (Fig. 3B and C).

3.3. CEP inhibits $HTNV_{pv}$ infection in the entry and membrane fusion phases

The entry process can be divided into receptor binding, receptor-mediated endocytosis and membrane fusion (Basu et al., 2011). To identify the phase of viral infection in which CEP acts, a time-of-addition
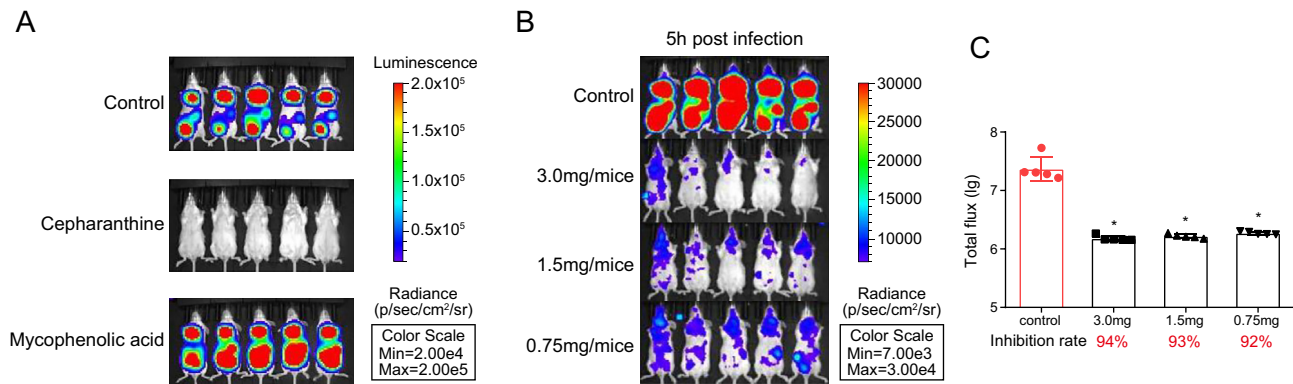
Fig. 3. Effect of Compounds on HTNV$_{pv}$ *in vivo*. **A** The BLI of CEP and mycophenolic acid treated mice. **B** The BLI of different concentrations of CEP treated mice. **C** The statistical analysis of the total flux of Fig. 3B. Female Balb/c mice (4–5 weeks old) were infected intraperitoneally with 4.2×10^5 TCID$_{50}$ HTNV$_{pv}$ (0 h). Compounds were delivered by IP injection to the Balb/c mice before infection (−6 h) and again 2 h after infection. Bioluminescence data were collected at 5 h after infection. Total flux (photons/s) due to luciferase expression in HTNV$_{pv}$ was measured with the bioluminescence imaging method. Statistical comparisons were made with a *t*-test. *$P < 0.05$, **$P < 0.01$, ***$P < 0.005$, and ****$P < 0.001$. Abbreviation: CEP, cepharanthine; MPA, Mycophenolic acid.

experiment was performed (Fig. 4A). Four stages of entry were examined as indicated. In this assay, a decrease of fluorescence in stage (a) suggests that the drug is a cell receptor antagonist, a decrease in stage (b) suggests that it is an inhibitor of viral entry, a decrease in stage (c) suggests that it is a membrane fusion inhibitor, and a decrease of fluorescence in stage (d) suggests that the drug is an inhibitor of viral replication after cell entry. Since replication cannot be tested using HTNV$_{pv}$, stage (d) was used as a negative control. It was therefore unclear whether the drug acts during the viral replication stage. The results shown in Fig. 4B indicate that CEP displayed only 33% inhibition of HTNV$_{pv}$ infection in stage (a), suggesting it is not a cell receptor antagonist. However, CEP inhibited HTNV$_{pv}$ infection by more than 70% during stages (b) and (c), suggesting that it may act during the entry phase and membrane fusion phase.

3.4. CEP inhibits authentic HTNV infection in vitro

When Vero E6 cells were infected with different titers of authentic HTNV, the nucleic acid copy number of HTNV was reduced by 73% in the cells treated with 20 μmol/L CEP compared to the control group (Fig. 5A). Different concentrations of CEP were then tested (Fig. 5B), and there was no inhibition below 6.6 μmol/L CEP. These results suggested

that the pseudotyped virus system is more sensitive to CEP than the authentic virus, since higher concentrations of CEP are needed in the latter.

4. Discussion

In this study, we screened 1813 approved drugs and 556 small-molecule compounds derived from traditional Chinese medicine sources, and identified one hit compound, CEP, that is effective against HTNV pseudovirus infection both *in vivo* and *in vitro*. CEP is a small-molecule compound from a traditional Chinese medicine source, mainly isolated from the plant *Stephania cephalantha* Hayata. CEP has been used to treat a variety of acute and chronic diseases for more than 70 years in Japan. It can be used to treat several acute and chronic diseases with few side effects (Bailly, 2019; Hong et al., 2015). We have demonstrated that CEP exerts activity against HTNV (EC$_{50}$ = 0.99 μmol/L, SI = 50). CEP not only displayed anti-HTNV activity *in vitro* but also inhibited HTNV-fluc infection in Balb/c mice. This compound has been reported to exert a broad spectrum of antiviral effects against human immunodeficiency virus 1 (HIV-1), SARS-CoV, Hepatitis B virus, and HSV-1 (Liu et al., 2004; Baba et al., 2001; Zhang et al., 2005; Zhou et al., 2012). The antiviral
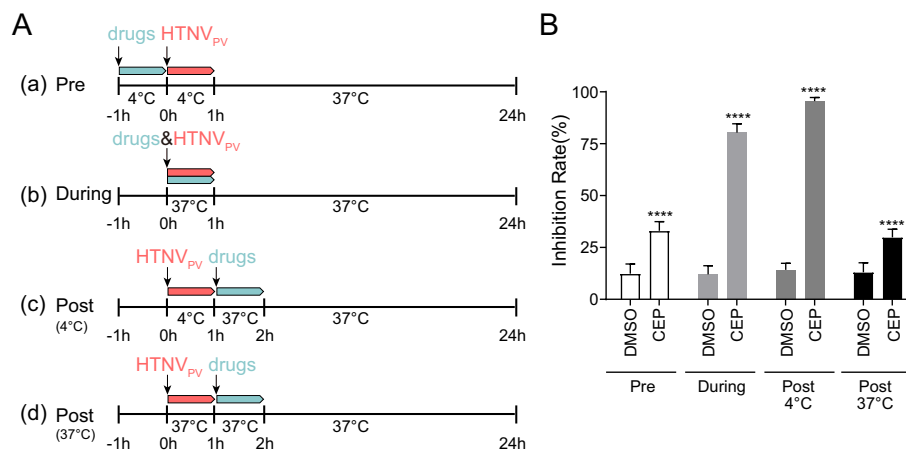

Fig. 4. Effects of CEP on different stages of HTNV$_{pv}$ entry. **A** Diagram of the time-of-addition experiment. This experiment determined the phase of infection in which the compound exerts its antiviral effect. Blue arrows show the period in which the compound was present. Red arrows show the periods in which HTNV$_{pv}$ was present. Vero E6 cells were infected with HTNV$_{pv}$ at different temperatures (4 °C or 37 °C) at time point 0 h for 1 h, and then washed three times with phosphate-buffered saline. CEP (30 μmol/L) was active at the indicated time points. Inhibition of HTNV$_{pv}$ infection was detected as the reduction in luciferase activity. **B** Inhibition rates of HTNV$_{pv}$ infection are presented as the means ± standard deviations of three independent experiments. CEP, cepharanthine; HTNV$_{pv}$, HTNV pseudovirus; DMSO, dimethyl sulfoxide.
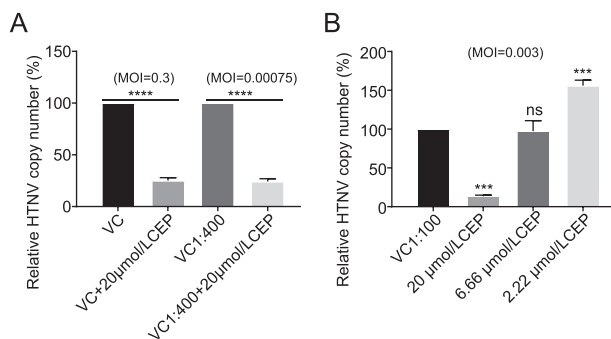
Fig. 5. Effects of CEP on authentic HTNV. **A** Vero E6 cells were infected with authentic HTNV(76–118 strain) at an MOI of 0.3 or 0.00075. The diluted CEP was added as indicated at a concentration of 20 μmol/L. **B** Vero E6 cells were infected with authentic HTNV at an MOI of 0.003. Different concentrations of CEP (20 μmol/L, 6.66 μmol/L, and 2.22 μmol/L) were added to the intervention group. The relative copy number of HTNV nucleic acid in the cells compared to the authentic HTNV group is shown. The data represent the means ± standard deviations from three independent experiments. VC: virus control group infected with authentic HTNV.

activity of CEP may be related to its inhibition of inflammatory cytokines and chemokines in cells.

In animal experiment, the compound was administered to Balb/c mice at 6 h before infection and 2 h after infection, and it inhibited $HTNV_{pv}$ infection by more than 90%. Therefore, CEP can be used as a preventive medication for HTNV infection. The other five compounds did not inhibit HTNV infection *in vivo*. Interestingly, MMF is a broad-spectrum antiviral drug (Diamond et al., 2002; Cho et al., 2017) that showed the highest anti-HTNV potency *in vitro* (SI > 900), but it did not show the expected efficacy *in vivo*. Factors such as the type of formulation, drug-enzyme interactions, or even interspecies differences in gastrointestinal absorption may explain this discrepancy. As Geisbert noted, many drugs act in cells but have no effect in rodents, or exert effects in rodents but not in monkeys (Enserink, 2014). These differences between species require further exploration. Ribavirin was also found to inhibit HTNV replication *in vitro* with an EC_{50} of 70 μmol/L (Huggins et al., 1984). More importantly, it was also shown to reduce the viral load and lethality in laboratory animals (Huggins et al., 1986). Nevertheless, clinical trials using ribavirin to treat hantavirus pulmonary syndrome failed to demonstrate sufficient efficacy compared to placebo-treated patients (Mertz et al., 2004). In our preliminary experiments, ribavirin was excluded because its EC50 against VSV/HTNVpv was over 10 μmol/L, which is much higher than the EC_{50} of CEP.

In a previous study, CEP was shown to inhibit the entry of HIV-1 by reducing the fluidity of the plasma membrane (Matsuda et al., 2014). To better understand the anti-HTNV mechanism of CEP, we performed a time-of-addition experiment (Fig. 4A), which showed that CEP affects the entry and membrane fusion phase of infection. In this study, we used $HTNV_{pv}$, which cannot replicate in cells. Therefore, CEP cannot inhibit stage (d), which would indicate the inhibition of replication after entry, and was used as a negative control group. It is also unclear whether the drug acts during the viral replication stage.

CEP was further tested against authentic HTNV infection *in vitro* with classical plaque reduction assay. However, no obvious inhibition of virus infection was observed (data not shown). We then analyzed the viral nucleic acid content of HTNV in infected cells. Treatment with 20 μmol/L CEP reduced the nucleic acid copy number of authentic HTNV infection at different MOIs (Fig. 5A), which suggested the drug is effective against authentic HTNV. And there was no inhibition effect below 6.6 μmol/L CEP (Fig. 5B). Interestingly, it seems that CEP may enhance the infection of HTNV at the low concentration of 2.22 μmol/L. Pseudovirus can only be used to examine the entry step of the infection, but more complicated steps are involved in the authentic virus infection. Further studies using

authentic HTNV in animal models are needed to evaluate the effects of CEP *in vivo*.

Here, we used $HTNV_{pv}$ to evaluate the antiviral effects of CEP *in vitro* and *in vivo*, and have presented a preliminary discussion of its antiviral mechanism. Another study reported that CEP interferes with the AMP-activated protein kinase (AMPK) and NF-κB signaling pathways (Bailly, 2019). This may indicate directions for our future research, to determine whether CEP inhibits HTNV by acting on these metabolic axes.

5. Conclusions

To identify anti-HTNV inhibitors, we established a high-throughput envelope-protein chimeric pseudoviral cell screening method, and used it to screen 1813 approved drugs and 556 small-molecule compounds derived from traditional Chinese medicine sources under BSL-2 conditions. Finally, six compounds were selected as anti-HTNV candidates at the cellular level, but only CEP was effective both *in vitro* and *in vivo*. The efficacy of CEP against HTNV has not been reported until now. It should be noted that the HTS performed in this study targeted the viral entry and membrane fusion phases rather than viral replication, because the pseudovirus is replication-deficient. Therefore, CEP is a candidate anti-HTNV drug, and our findings should lead to the development of new antiviral drugs that are efficacious against hantaviruses.

References

Augello, G., Modica, M., Azzolina, A., Puleio, R., Cassata, G., Emma, M.R., Di Sano, C., Cusimano, A., Montalto, G., Cervello, M., 2018. Preclinical evaluation of antitumor activity of the proteasome inhibitor MLN2238 (ixazomib) in hepatocellular carcinoma cells. Cell Death Dis. 9, 28.

Avsic-Zupanc, T., Saksida, A., Korva, M., 2019. Hantavirus infections. Clin. Microbiol. Infect. 21S, e6–e16.

Baba, M., Okamoto, M., Kashiwaba, N., Ono, M., 2001. Anti-HIV-1 activity and structure-activity relationship of cepharanoline derivatives in chronically infected cells. Antivir. Chem. Chemother. 12, 307–312.

Bailly, C., 2019. Cepharanthine: an update of its mode of action, pharmacological properties and medical applications. Phytomedicine 62, 152956.

Basu, A., Li, B., Mills, D.M., Panchal, R.G., Cardinale, S.C., Butler, M.M., Peet, N.P., Majgier-Baranowska, H., Williams, J.D., Patel, I., Moir, D.T., Bavari, S., Ray, R., Farzan, M.R., Rong, L., Bowlin, T.L., 2011. Identification of a small-molecule entry inhibitor for filoviruses. J. Virol. 85, 3106–3119.

Brocato, R.L., Hooper, J.W., 2019. Progress on the prevention and treatment of hantavirus disease. Viruses 11, 610.

Cho, J., Yi, H., Jang, E.Y., Lee, M.S., Lee, J.Y., Kang, C., Lee, C.H., Kim, K., 2017. Mycophenolic mofetil, an alternative antiviral and immunomodulator for the highly pathogenic avian influenza H5N1 virus infection. Biochem. Biophys. Res. Commun. 494, 298–304.

Diamond, M.S., Zachariah, M., Harris, E., 2002. Mycophenolic acid inhibits dengue virus infection by preventing replication of viral RNA. Virology 304, 211–221.

Engur-Ozturk, S., Dikmen, M., 2022. Proteasome inhibitor immunotherapy for the epithelial to mesenchymal transition: assessing the A549 lung cancer cell microenvironment and the role of M1, M2a and M2c 'hydrocortisone-polarised' macrophages. Mol. Biol. Rep. https://doi.org/10.1007/s11033-022-07329-w.

Enserink, M., 2014. Infectious diseases. Debate erupts on 'repurposed' drugs for Ebola. Science 345, 718–719.

Grad, I., Hanes, R., Ayuda-Duran, P., Kuijjer, M.L., Enserink, J.M., Meza-Zepeda, L.A., Myklebost, O., 2021. Discovery of novel candidates for anti-liposarcoma therapies by medium-scale high-throughput drug screening. PLoS One 16, e0248140.

Hong, L., Guo, Z., Huang, K., Wei, S., Liu, B., Meng, S., Long, C., 2015. Ethnobotanical study on medicinal plants used by Maonan people in China. J. Ethnobiol. Ethnomed. 11, 32.

Hong, X., Chen, Z., Guo, Y., Dong, Y., He, X., Chen, M., Ju, W., 2022. Combined liver, pancreas-duodenum, and kidney transplantation for patients with hepatitis B cirrhosis, uremia, and insulin-dependent diabetes. Ann. Transplant. 27, e935860.

Huggins, J.W., Kim, G.R., Brand, O.M., McKee, K.J., 1986. Ribavirin therapy for Hantaan virus infection in suckling mice. J. Infect. Dis. 153, 489–497.

Huggins, J.W., Robins, R.K., Canonico, P.G., 1984. Synergistic antiviral effects of ribavirin and the C-nucleoside analogs tiazofurin and selenazofurin against togaviruses, bunyaviruses, and arenaviruses. Antimicrob. Agents Chemother. 26, 476–480.

Jin, Y.H., Kwon, S., Choi, J.G., Cho, W.K., Lee, B., Ma, J.Y., 2019. Toosendanin from melia fructus suppresses influenza A virus infection by altering nuclear localization of viral polymerase PA protein. Front. Pharmacol. 10, 1025.

Jonsson, C.B., Figueiredo, L.T., Vapalahti, O., 2010. A global perspective on hantavirus ecology, epidemiology, and disease. Clin. Microbiol. Rev. 23, 412–441.

Kariwa, H., Yoshimatsu, K., Arikawa, J., 2007. Hantavirus infection in East Asia. Comp. Immunol. Microbiol. Infect. Dis. 30, 341–356.

Liu, X., Wang, Y., Zhang, M., Li, G., Cen, Y., 2004. Study on the inhibitory effect of cepharanthine on herpes simplex type-1 virus (HSV-1) *in vitro*. Zhong Yao Cai 27, 107–110 (in Chinese).

Llah, S.T., Mir, S., Sharif, S., Khan, S., Mir, M.A., 2018. Hantavirus induced cardiopulmonary syndrome: a public health concern. J. Med. Virol. 90, 1003–1009.

Matsuda, K., Hattori, S., Komizu, Y., Kariya, R., Ueoka, R., Okada, S., 2014. Cepharanthine inhibited HIV-1 cell-cell transmission and cell-free infection via modification of cell membrane fluidity. Bioorg. Med. Chem. Lett 24, 2115–2117.

Mercorelli, B., Palu, G., Loregian, A., 2018. Drug repurposing for viral infectious diseases: how far are we? Trends Microbiol. 26, 865–876.

Mertz, G.J., Miedzinski, L., Goade, D., Pavia, A.T., Hjelle, B., Hansbarger, C.O., Levy, H., Koster, F.T., Baum, K., Lindemulder, A., Wang, W., Riser, L., Fernandez, H., Whitley, R.J., 2004. Placebo-controlled, double-blind trial of intravenous ribavirin for the treatment of hantavirus cardiopulmonary syndrome in North America. Clin. Infect. Dis. 39, 1307–1313.

Milholland, M.T., Castro-Arellano, I., Suzan, G., Garcia-Pena, G.E., Lee, T.J., Rohde, R.E., Alonso, A.A., Mills, J.N., 2018. Global diversity and distribution of hantaviruses and their hosts. EcoHealth 15, 163–208.

Montoya-Ruiz, C., Diaz, F.J., Rodas, J.D., 2014. Recent evidence of hantavirus circulation in the American tropic. Viruses 6, 1274–1293.

Ning, T., Wang, L., Liu, S., Ma, J., Nie, J., Huang, W., Li, X., Li, Y., Wang, Y., 2021. Monitoring neutralization property change of evolving hantaan and Seoul viruses with a novel pseudovirus-based assay. Virol. Sin. 36, 104–112.

Pushpakom, S., Iorio, F., Eyers, P.A., Escott, K.J., Hopper, S., Wells, A., Doig, A., Guilliams, T., Latimer, J., McNamee, C., Norris, A., Sanseau, P., Cavalla, D., Pirmohamed, M., 2019. Drug repurposing: progress, challenges and recommendations. Nat. Rev. Drug Discov. 18, 41–58.

Sohraby, F., Bagheri, M., Aliyar, M., Aryapour, H., 2017. In silico drug repurposing of FDA-approved drugs to predict new inhibitors for drug resistant T315I mutant and wild-type BCR-ABL1: a virtual screening and molecular dynamics study. J. Mol. Graph. Model. 74, 234–240.

Tian, H., Stenseth, N.C., 2019. The ecological dynamics of hantavirus diseases: from environmental variability to disease prevention largely based on data from China. PLoS Neglected Trop. Dis. 13, e0006901.

Wang, H., Yu, Y., Jiang, Z., Cao, W.M., Wang, Z., Dou, J., Zhao, Y., Cui, Y., Zhang, H., 2016. Next-generation proteasome inhibitor MLN9708 sensitizes breast cancer cells to doxorubicin-induced apoptosis. Sci. Rep. 6, 26456.

Yap, D.Y.H., Li, P.H., Tang, C., So, B.Y.F., Kwan, L.P.Y., Chan, G.C.W., Lau, C.S., Chan, T.M., 2022. Long-term results of triple immunosuppression with tacrolimus added to mycophenolate and corticosteroids in the treatment of lupus nephritis. Kidney Int. Rep. 7, 516–525.

Ye, L., Li, J., Zhang, T., Wang, X., Wang, Y., Zhou, Y., Liu, J., Parekh, H.K., Ho, W., 2012. Mycophenolate mofetil inhibits hepatitis C virus replication in human hepatic cells. Virus Res. 168, 33–40.

Zhang, C.H., Wang, Y.F., Liu, X.J., Lu, J.H., Qian, C.W., Wan, Z.Y., Yan, X.G., Zheng, H.Y., Zhang, M.Y., Xiong, S., Li, J.X., Qi, S.Y., 2005. Antiviral activity of cepharanthine against severe acute respiratory syndrome coronavirus in vitro. Chin. Med. J. (Engl.) 118, 493–496.

Zhang, J.H., Chung, T.D., Oldenburg, K.R., 1999. A simple statistical parameter for use in evaluation and validation of high throughput screening assays. J. Biomol. Screen 4, 67–73.

Zhang, L., Li, Q., Liu, Q., Huang, W., Nie, J., Wang, Y., 2017. A bioluminescent imaging mouse model for Marburg virus based on a pseudovirus system. Hum. Vaccines Immunother. 13, 1811–1817.

Zhang, T.T., Huang, Z.T., Dai, Y., Chen, X.P., Zhu, P., Du, G.H., 2006. High-throughput fluorescence polarization method for identifying ligands of LOX-1. Acta Pharmacol. Sin. 27, 447–452.

Zhou, Y.B., Wang, Y.F., Zhang, Y., Zheng, L.Y., Yang, X.A., Wang, N., Jiang, J.H., Ma, F., Yin, D.T., Sun, C.Y., Wang, Q.D., 2012. In vitro activity of cepharanthine hydrochloride against clinical wild-type and lamivudine-resistant hepatitis B virus isolates. Eur. J. Pharmacol. 683, 10–15.